Journal of
Synchrotron Radiation

ISSN 0909-0495

Received 19 June 2009
Accepted 17 December 2009

Manganese speciation in *Diplodon chilensis patagonicus* shells: a XANES study

A. L. Soldati,[a]* J. Goettlicher,[b] D. E. Jacob[a] and V. Vicente Vilas[c]

[a]Department of Geosciences, and Earth System Science Research Centre, Johannes Gutenberg-University, Mainz, Germany, [b]Institute for Synchrotron Radiation (ISS), Forschungszentrum Karlsruhe, Eggenstein-Leopoldshafen, Germany, and [c]Catholic University of Valencia, Faculty of Medicine, Valencia, Spain. E-mail: soldatia@uni-mainz.de

X-ray absorption near-edge spectroscopy (XANES) at the Mn *K*-edge was used to investigate the environment of Mn *in situ* within the growth increments of the long-lived freshwater bivalve species *Diplodon chilensis patagonicus*. Single XANES spectra and Mn $K\alpha$ fluorescence distributions were acquired at submillimetre resolution (up to 100 μm × 50 μm), at Mn concentrations below the weight percent range (100–1000 μg g^{-1}) in a high Ca matrix. The position and intensity of the pre-edge feature in the shell spectrum resembles best that of the Mn(II)-bearing reference compounds, suggesting that this is the oxidation state of Mn in the bivalve shells. By comparison with the XANES spectra of selected standard compounds, hypotheses about Mn speciation in the shell are also reported. In particular, different factors, such as provenance, ontogenetic age, variable Mn-concentrations or seasonal shell deposition seem not to influence the speciation of the metal in this bivalve species.

Keywords: bivalve shell; biomineralization; manganese; speciation; XANES.

1. Introduction

The freshwater bivalve *Diplodon chilensis patagonicus* is a long-living species, widely distributed in lakes and rivers in southern South America (Castellanos, 1959, 1960). As in many other bivalves (Rosenberg & Jones, 1975), trace elements are incorporated periodically into the shell carbonate of *Diplodon ch. patagonicus* (Soldati *et al.*, 2009) and could be potentially transformed into a natural proxy archive of the environment or ecosystem history. In turn, environmental parameters such as ambient temperature, precipitation gradients, seawater salinity and primary production influence the elemental composition of the biogenic carbonate (Lutz & Rhoads, 1980; Rosenberg, 1980). In the case that so-called vital effects (Urey *et al.*, 1951) can be excluded or corrected for (Lorrain *et al.*, 2005; Carré *et al.*, 2006; Gillikin *et al.*, 2006), environmental parameters can be evaluated or reconstructed from the shells by means of sclerochronological and geochemical methods (*e.g.* Klein *et al.*, 1996*a*,*b*; Toland *et al.*, 2000; Van der Putten *et al.*, 2000; Schöne *et al.*, 2005).

Because of their long life spans, some bivalve species are especially interesting for these kinds of studies. Indeed, *Diplodon ch. patagonicus* individuals can have life spans of more than 90 years (Soldati *et al.*, 2009) and studies of some unionid populations showed that individuals reach ages in excess of a century (Anthony *et al.*, 2001). Thus, the valves of these animals contain environmental information of many decades, periodically archived and annually and sometimes even seasonally resolved (*i.e.* Tevesz & Carter, 1980; Parada *et al.*, 1989; Semenas & Brungi, 2002; Valdovinos & Pedreros, 2007).

Mg/Ca, Sr/Ca, Mn/Ca and Ba/Ca ratios in the shells of freshwater and marine bivalves are good examples of elements with potential to be used as proxies (*i.e.* Lazareth *et al.*, 2003; Klein *et al.*, 1996*a*; Freitas *et al.*, 2006, 2009; Wanamaker *et al.*, 2008). However, all of these assume that the X^{2+} ion is replacing the Ca^{2+} ion in the carbonate structure, which may not always be the case (Dodd, 1967; Rosenberg, 1980; Lingard *et al.*, 1992). Trace elements in calcareous skeletons may also occur as separate phases adsorbed onto crystal surfaces or as forming part of organic compounds as pigments or shell proteins (Comfort, 1951; Fox, 1966; Dodd, 1967; Soldati *et al.*, 2007).

New findings demonstrated that the metal speciation in shells depends highly on the bivalve species studied. The element magnesium is a good example: Mg incorporation into biogenic carbonate is controlled by the temperature of precipitation as well as the concentration of Mg in the water (Lorens & Bender, 1980). Therefore, many efforts focus to establish this element as a proxy for temperature in different bivalves. However, Mg^{2+} is not always simply replacing the Ca^{2+} ion in the carbonate structure. For example, Foster *et al.* (2008) showed that Mg is probably bound to organic molecules in *Arctica islandica*, while Clarke *et al.* (2009) demonstrated that it is hosted in a calcite-type phase in *Pecten maximus*, but predominantly in an organic phase in *Mytilus*

edulis. Physiologically, Mg ions associated with an organic environment play an essential role as active sites in specific proteins or as biocatalyst for enzymatic as well as anti-oxidative processes (Rosenberg *et al.*, 2001; Haraguchi, 2004). As is typical for freshwater environments, the shells studied here have Mn concentrations that exceed those of Mg by orders of magnitude (Soldati *et al.*, 2009), whereas Mg is much more abundant in marine shells. Furthermore, there is evidence that Mn is able to replace Mg as a biometal in physiological processes (*e.g.* Maguire & Cowan, 2002). However, it remains unknown as to whether Mn in *Diplodon* shells replaces Ca^{2+} in aragonite or if it is hosted by the organic phase present in all bivalve shells.

The presence of manganese in tissues and shells of freshwater bivalves has been known for around a century (Bradley, 1910; Boycott, 1921). High abundances in muscle tissues and organs suggest some fundamental role of Mn in the animal's metabolism (Bradley, 1910) and correlate with Mn content in water. Later studies showed that environmental factors like temperature and salinity influence the total Mn content found in shells of different marine molluscs (Pilkey & Goodell, 1963; Gordon *et al.*, 1970). More recently, spatial high-resolution techniques allowed the determination of Mn concentration patterns in many species (*i.e.* Carriker *et al.*, 1982; Barbin *et al.*, 1995). Indeed, variable Mn concentrations in the shells of some freshwater bivalve species are often related to differences in environmental parameters (Siegele *et al.*, 2001). Jeffree *et al.* (1995), for example, showed that micro-laminations in the valves of the freshwater hyriid *Hyridella depressa* were a long-term monitor for Mn concentration in the water. Langlet *et al.* (2006) demonstrated that seasonal trends of Mn/Ca ratios in valves of the freshwater bivalve *Pleiodon spekii* matched the seasonal increase in chlorophyll-a concentration in surface waters of Lake Tanganyika, which is associated with the monsoon climate system. High-resolution *in situ* trace-elemental analyses in shells of *Diplodon* (Soldati *et al.*, 2009) show that Mn is precipitated in cyclic annual patterns, with higher concentrations in summer and lower concentrations in winter growth increments; in analogy with the seasonal fluctuations of chlorophyll-a contents in the water body (Queimaliños, 1997). Thus, Mn-concentrations in *Diplodon* shells could potentially be used as proxy for the primary productivity in Patagonian lakes.

Some pioneering works dealt with the incorporation mechanisms and chemical characteristics of Mn in bivalve shells. Allen (1960), for example, reported Mn-rich deposits on the surface of a variety of marine molluscs and concluded that Mn^{2+} exchanges with Ca^{2+} in the $CaCO_3$ structure of the shell. Swinehart & Smith (1979) found that Mn^{2+} is deposited in the periostracum (the outermost organic layer, Fig. 1*b*) of *Anodonta californiensis* and *Unio novahollandae* and proposed that it replaces Ca^{2+} in the $Ca_3(PO_4)_2$ detected in the periostracum layer of these species. They further reported on potential contributions of Mn(IV) (as MnO_2) in electro-spin resonance spectra; surface adsorption/desorption mechanisms were observed to occur between the periostracum and the surrounding media, and were proposed as the main uptake path of Mn into the organic tissue. Using electron paramagnetic resonance, Naidu *et al.* (1992) reported octahedral symmetry for Mn(II) in shells of *Lamillidens marginallis*. Narasimhulu & Rao (2000) studied *Mytilus conradinus* and reported Mn(II) in the nacreous layer (Fig. 1*a*), while Mn(III) was found to be present in the prismatic layer (Fig. 1*a*). Carriker *et al.* (1980) proposed that Mn found in the prismatic layer of *Cassostrea virginica* was associated with the organic matrix, as it was found to be more abundant in this layer than in the rest of the shell. Similarly, Takesue *et al.* (2008) argued that a major part of Mn is hosted by an organic phase in *Corbula amurensis*.

In an earlier study, it was shown that the annual growth line in *Diplodon chilensis patagonicus* is formed in the austral spring (Soldati *et al.*, 2009). The shell material deposited during this period has a higher organic to mineral ratio and coincides with the highest measured Mn concentrations in one annual shell increment. This implies that a major part of the Mn budget could be bound organically in *Diplodon* shells, in analogy to Mg in *Mytilus edulis*. Here, we test this hypothesis using X-ray absorption near-edge structure (XANES) on the sub-millimetre scale to analyze the Mn environment in different shells and in structurally different parts of one shell. The results are compared with Mn in different organic and inorganic reference samples to elucidate the possible Mn speciation in this biocarbonate.

2. Methodology

2.1. Shell structure

Shells of *Diplodon ch. patagonicus* consist of different layers (Fig. 1*a*). The outermost layer is a brownish organic tissue, the periostracum (Fig. 1*b*). The inside of the valve is composed of a thin prismatic layer of about 200 µm and a thick nacre layer of some millimetres thickness (Fig. 1*b*) towards the soft body. The nacre layer can be subdivided into an 'external' (adjacent to the prismatic layer) and 'internal' (in contact with the soft body of the animal) layer. Both prism and nacre layers are made of calcium carbonate ($CaCO_3$) in the form of aragonite as verified by Raman spectroscopic analyses (Soldati *et al.*, 2009).

A polished transversal section through the shell following the minimal growth axis shows the presence of alternating light/dark bands, well observable in the external nacre layer (Fig. 1*a*, left). Each pair of bands corresponds to one year: the light band is deposited during the cold season and the darker band during the summer (Fig. 1*c*; Parada *et al.*, 1989; Soldati *et al.*, 2009).

After treatment with *Alcian blue* (see Soldati *et al.*, 2009 for details), sharp blue lines are highlighted in the shell cross section (Fig. 1*d*). These lines are the growth lines that form during late spring, and thus can be used to define the temporal growth scale for the shell. Biologically, the formation of the line in this species is associated with a period of very slow shell growth (or sometimes even growth stop) and is related to the reproduction period.

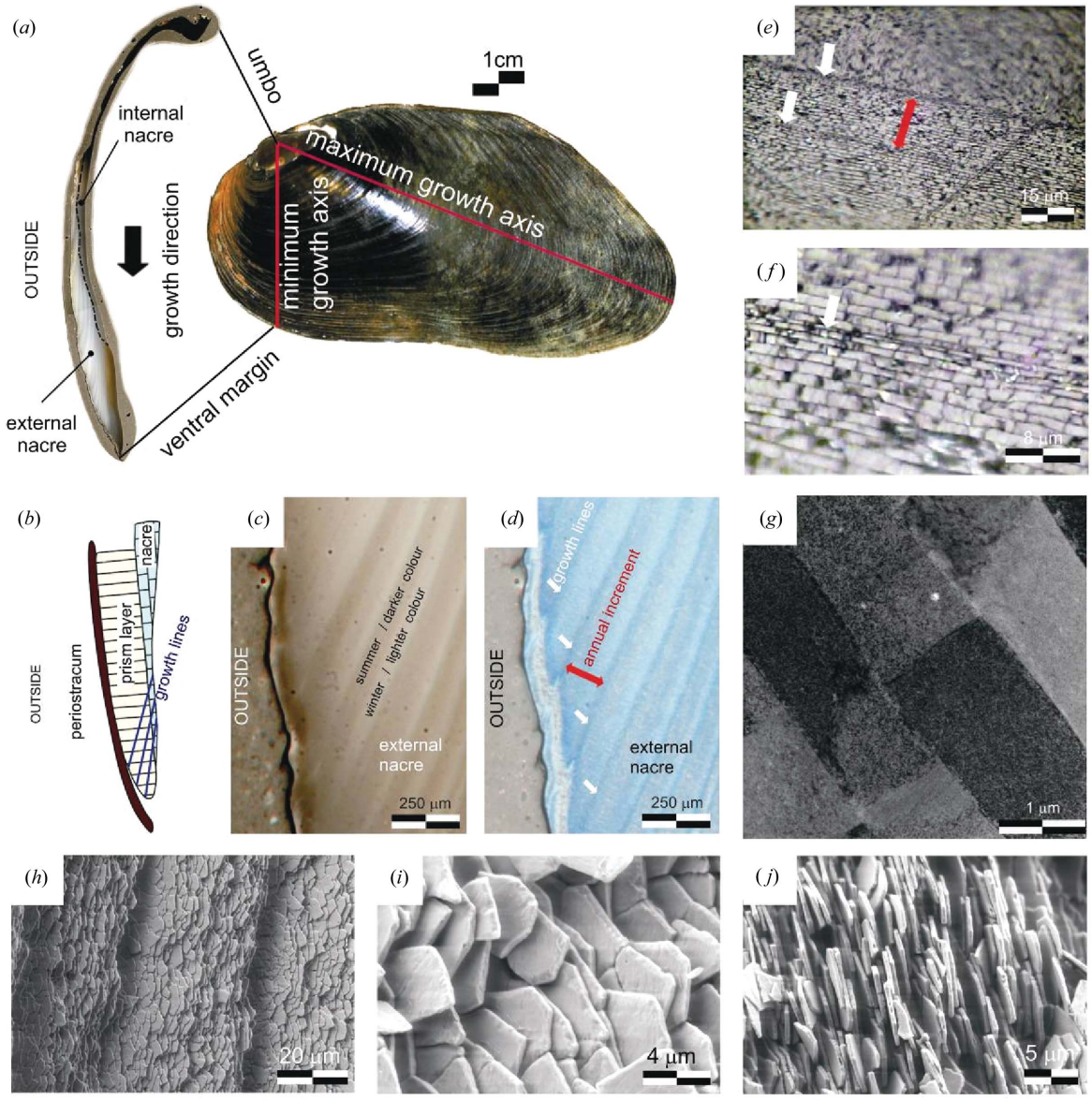

Figure 1
(*a*) Right valve of a *Diplodon ch. patagonicus* individual showing different shell structures; a transversal cross section along the minimal growth axis (enlarged) is shown on the left (modified from Soldati *et al.*, 2009). (*b*) Schematic of a shell cross section showing the structural components of a *Diplodon* valve (not to scale). Reflected light microscopic image showing pairs of light/dark (winter/summer) banding corresponding to one annual increment (*c*) and highlighted blue (using *Alcian blue*) annual growth lines (white single arrow, *d*) dividing each annual growth increment (red double arrow). (*e* and *f*) Reflected light confocal microscopy shows that the growth lines (white arrows) are formed by thinner layers of platelets than during the rest of the year (*f*). (*g*) Dark-field transmission electron microscopy image of the nacre platelets in a focused ion beam polished sample; image perpendicular to the *c*-axis of the aragonite platelets. (*h*–*j*) Scanning electron microscopy images of a fractured piece of shell showing that the annual increments (*h*) and the nacre platelets are almost arranged parallel (*i*) with their base plane perpendicular (*j*) to the crystallographic *c*-axis of the crystals.

The target of the present study was the 'external' part of the nacre layer (Fig. 1*b*), where the growth lines are better observed (Figs. 1*a* and 1*d*). The structure of the external nacre layer (Fig. 1*g*) is often referred to as being reminiscent of a brick wall, where the bricks are the polygonal aragonite platelets bound together by the interlamellar organic matrix functioning as mortar (*e.g.* Erben & Watabe, 1974). Reflected light microscopy at higher magnification demonstrates that the nacre platelets in this region are thinner than those deposited during the remaining year (Figs. 1*e* and 1*f*), while the organic interlamellar sheets retain their usual thickness. During this period the mineral to organic ratio in the nacre decreases and the lines can be highlighted by dyeing with *Alcian Blue* (Fig. 1*d*). In the following we will refer to these regions as the annual growth lines or growth lines of the shell. The aragonite platelets are flat polygonal structures of about 5–7 µm in diameter and ~1.5–0.5 µm thickness (Figs. 1*h*–1*j*). They consist of highly aligned aragonite nano-crystals, intergrown with an intra-crystalline organic material and oriented with their crystallographic *c*-axes perpendicular to the surface of the shell (Erben & Watabe, 1974).

2.2. Sample preparation

Diplodon bivalves were captured alive in March 2007 in lakes and rivers of the Nahuel Huapi National Park and its surroundings (40°S 71°W, Patagonia, Argentina). The mussels were sacrificed immediately and the soft parts removed. The shells were washed with distilled water, cleaned with a brush and air dried. The left valves were covered with an epoxy resin (WIKO, Greussenheim, Germany) on the inner and the outer side, to provide a better material resistance during subsequent cutting. Two samples (AS07RM0018 from River Manso Inferior and AS07LS0026 from Lake Steffen) were selected for XANES analysis. One slab of 3 mm width was cut with a low-speed saw (Buehler, IL, USA) from each shell following the minimal growth axis perpendicular to the growth rings (Fig. 1*a*). The slabs were ground on glass plates with SiC powder and polished with Al_2O_3 on Buehler G-cloths. After this treatment the samples were rinsed three times with MilliQ water for 3 min in an ultrasonic bath and air dried before measurement.

Table 1
Organic and inorganic reference materials used in this work.

Compound		Oxidation state	Purity	Source
Mn metallic	Mn	Mn(0)	>99.99%	Riedel-de-Haën
Mn sulfate	$MnSO_4{\cdot}H_2O$	Mn(II)	>99%	Merck
Mn nitrate	$Mn(NO_3)_2{\cdot}4\ H_2O$	Mn(II)	>97%	Fluka Analytical
Mn carbonate (calcite structure)	$MnCO_3$	Mn(II)	>97%	Sigma Aldrich
Mn dioxide	MnO_2	Mn(IV)	85–90%	Merck Chemicals
Potassium permanganate	$KMnO_4$	Mn(VII)	>99%	Merck Chemicals
Mn acetate tetrahydrate	$Mn(CH_3CO_2)_2{\cdot}4\ H_2O$	Mn(II)	>97%	Merck Chemicals
Mn porphine	$C_{44}H_{28}ClMnN_4$	Mn(III)	95%	Sigma Aldrich
Aragonite crystal†	Mn traces in $CaCO_3$	Mn(II)	Traces	–
Diplodon periostracum	Unknown	Unknown	Traces	–

† The aragonite sample is a specimen from Mina Sal, Cuenca, Spain, from the Mineral Collection of the Department of Geosciences, Johannes Gutenberg-University of Mainz.

2.3. X-ray fluorescence and XANES analyses

X-ray fluorescence mapping for Mn distribution in the shells (step size typically 70 µm × 50 µm) and Mn *K*-edge XANES measurements were carried out at the X-ray beamline of the Synchrotron Radiation Laboratory for Environmental Studies of the synchrotron radiation source ANKA (Forschungszentrum Karlsruhe, Germany; SUL-X, 2009) using a double-crystal monochromator with Si(111) crystals and Kirkpatrick–Baez focusing.

Prior to XANES spectroscopy the shell samples were mapped with the intensity of the Mn *Kα* fluorescence emission line in order to locate the Mn-rich/Mn-poor areas of interest. Beam size in this modus was about 70 µm × 50 µm on the sample, and the maps were acquired with overlapping spots. The Mn *Kα* emission lines at about 5900 eV were excited at 6550 and 6800 eV. Excitation at 6550 eV results in enhanced fluorescence intensity because it is close to the energy of the white line and is therefore better suited for mapping of low Mn contents.

Mn *K*-edge XANES spectra were then recorded at selected positions in an energy range from 6389 eV (about 150 eV prior to the absorption edge) to at least 6850 eV above the edge (step width $k = 0.05$) to have sufficient data ranges for pre- and post-edge background subtraction. Across the edge energy of about 6539 eV, steps of 0.3 eV were chosen to have sufficient resolution for the XANES resonances.

Because of the low Mn concentrations in the sub-percentage range, XANES spectra were recorded in fluorescence mode with a seven-element Si(Li) solid-state detector. The same detector was used for the signal detection during fluorescence mapping. Beam and detector were positioned in a 90° configuration. The sample was orientated at about 45° to the beam direction and the detector axis.

Polished shell samples were measured directly or covered with a 50 µm Kapton foil to reduce the *Kα* fluorescence signal of Ca. The beam energy in micro-focus mode was calibrated once a day before the start of the measurements; a Mn(0) reference was measured simultaneously with the samples for spectral calibration. The energy was calibrated to 6539 eV for the maximum of the first derivative of the Mn(0) reference foil. Beam size on the samples was 100 µm × 50 µm for most cases and is specified in each figure.

For data evaluation, XANES spectra of reference substances were measured in order to obtain first implications towards Mn valence and bonding. References used are listed in Table 1 and comprise Mn-metal, Mn-sulfate, -nitrate, -carbonate and -dioxide, Mn in organic compounds (Mn-porphine and Mn-acetate), Mn traces in natural aragonite crystals, and a dry piece of tissue from the shell periostracum. X-ray powder diffractometry (XRD) analyses show that all the chemical compounds used as references have a well crystallized structure. Contrary, the periostracum shows a high amorphous fraction from XRD. The aragonite crystal, the shell cross sections and the periostracum were measured *in situ* without any previous treatment; the other reference materials were powdered, homogenized and mixed with polyethylene. Powder pellets were prepared under N_2 atmosphere applying a pressure of 5 tons cm^{-2} for 2 min. All measurements were triplicated with an acquisition time of 1 s per energy or *k* step for the references and 3 s for the shell sample. For the pure Mn compounds, XANES spectra were measured in transmission and fluorescence mode. Transmission spectra were preferred because of self-absorption effects in the fluorescence mode which are difficult to correct for. Data were evaluated using *Athena* from the *IFEFFIT* package (Ravel & Newville, 2005).

3. Results and discussion

In situ Mn *Kα* X-ray fluorescence maps of the lake (Fig. 2*a*) and of the river sample (Fig. 2*b*) show the presence of well resolved alternating lines of high and low Mn concentrations

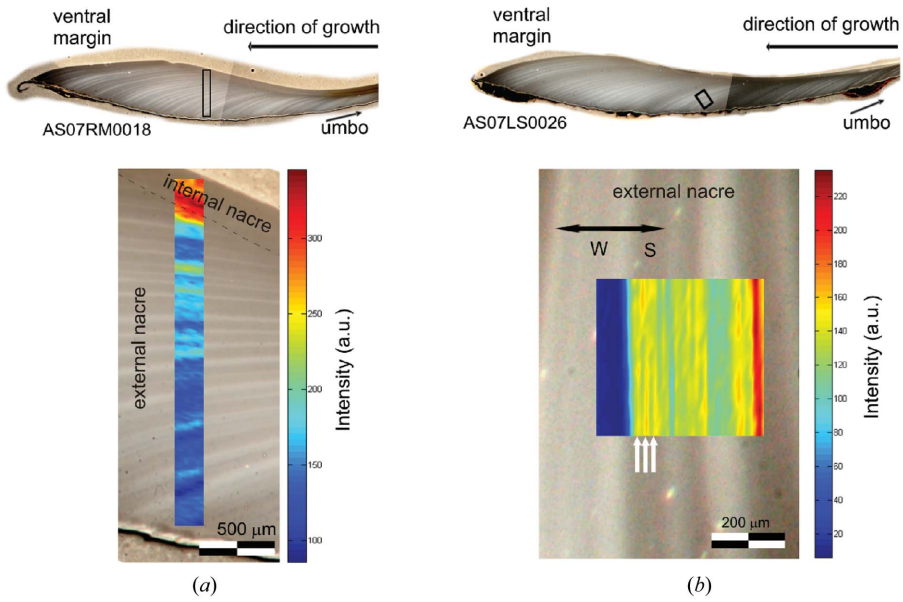

(*a*) (*b*)

Figure 2
Shell cross section showing the light/dark (winter/summer) banding and corresponding Mn X-ray fluorescence map of a *Diplodon* shell from River Manso Inferior (*a*) and from Lake Steffen (*b*). The black frames in the photographs show the region of mapping; this region is shown enlarged at the bottom at the same scale as the fluorescence map: higher concentrations of Mn are found in the darker bands of the external nacre in both shells and in the portion of internal nacre mapped in (*a*). Beam size on the sample was 70 µm × 50 µm; a.u.: arbitrary units. In (*b*), double arrow = one year; w = winter; s = summer; single arrows = intra-annual variations.

that follow the growth increments of the shell. Supporting previous investigations (Soldati *et al.*, 2009), higher concentrations of manganese (400–800 µg g^{-1}) were found in the summer increments (dark bands in the cross sections in Figs. 2*a* and 2*b*) and near the annual growth line, while lower Mn concentrations (100–300 µg g^{-1}) were found in the winter increments (light bands). Furthermore, higher Mn concentrations were found in the 'internal' part of the nacre layer, but alternating Mn concentration banding is not so clear for this portion of the shell (Fig. 2*a*). The widest Mn-rich areas detected in the external nacre layer are about 250 µm in thickness. Regions with intermediate Mn concentrations inside these Mn-rich areas were also observed (Fig. 2*b*, white arrows) and might be related to unresolvable intra-annual microlaminations.

Three spots with high, medium and low Mn concentrations were selected from the map in Fig. 2(*b*) and the Mn *K*-edge absorption spectra in the XANES region were measured there using a focused beam with 100 µm × 50 µm spot size on the sample. The three micro-XANES spectra (Fig. 3*a*) show no visible difference: pre-edge peak position and intensity, Mn-edge inflection point and crest, and spectral form are identical suggesting that within the spatial resolution of the measurement of 50 to 100 µm the structural environment of the Mn atom does not change and thus does not depend on the Mn concentration in the shell. In the same sample, a spot of high Mn concentration within the adult section of the shell (near the ventral margin) and one deposited at younger age (near the umbo region) were compared. Also, in this case the micro-XANES spectra (Fig. 3*b*) show identical features, suggesting that the ontogenetic age of the mussel does not play an important role in the speciation of Mn in the shell.

In order to investigate possible relations of the Mn speciation with sample provenance, one spot in the river sample was compared with a similar spot in the lake sample (both in adult regions, in a band with high concentration). No differences could be detected between the XANES spectra (Fig. 3*c*). Thus, all single spots analyzed here show the same spectral features independent of the position in the shell, season of deposition, distance to the growth line or provenance of the sample. In the following, these are called the 'shell' spectra.

A piece of periostracum tissue was analyzed as reference for the organic material and a fragment of a natural aragonite crystal with Mn traces (Table 1) was used as reference for the pure mineral part. Both XANES spectra are compared with the shell spectra in Fig. 3(*d*). According to the spectra, the environment of the Mn atom in the shell differs both from that of the organic component of the same shell (periostracum) and from that of crystal aragonite. The shell spectrum shows a secondary peak after the main resonance (white line) at ∼6564 eV (*b* in Fig. 3*d*), while the spectrum of the periostracum is characterized by a smooth curve without a peak. The spectrum of Mn-containing aragonite has a shoulder peak in this range at distinctively lower energies (∼6560 eV). However, the Mn *K*-edge inflection point occurs at almost the same position in all three samples and the maximum of the white line (line *a* in Fig. 3*d*) occurs within 1.2 eV suggesting the same Mn valence, *i.e.* Mn(II), for shell and periostracum as in Mn-containing aragonite. An interesting corollary of this measurement is that the spectrum of the periostracum sample shows very similar features as that of the aragonite crystal (Fig. 3*d*), suggesting that Mn in the organic tissue could be Mn(II) with a similar near-neighbour structure as Mn in aragonite. Indeed, diluted Mn(II) occupying an octahedral field was reported in the periostracum of *Unio novahollandae*, another unionid freshwater bivalve (Swinehart & Smith, 1979). In this case it was found that Mn^{2+} is replacing the Ca^{2+} ion in $Ca_3(PO_4)_2$. Comparison of our XANES periostracum spectrum (Fig. 3*d*) with published spectra of Mn-phosphates (Nietubyć *et al.*, 2001) shows the main resonance peak as a double peak at higher energies (6548 eV) distinctly different from that of the periostracum spectrum. This, and the fact that *Diplodon* shells have very low P content (Soldati *et al.*, 2009), suggests that Mn-phosphates do not play a role in the periostracum of this bivalve species. Swinehart & Smith (1979) further speculated on a potential contribution of Mn(IV) as MnO_2 in the perio-

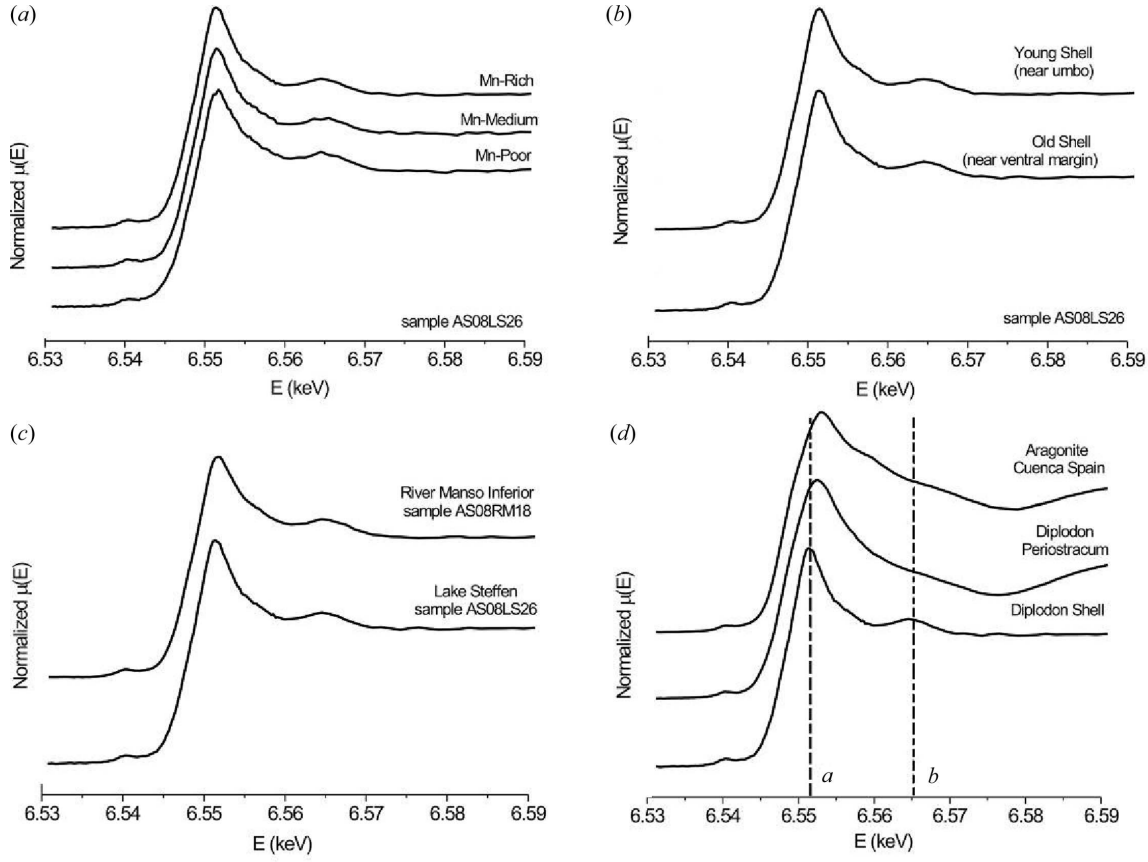

Figure 3
X-ray absorption spectra from *in situ* analyses of shells and reference materials. The spectra are normalized between 0 and an edge jump of 1 and shifted vertically for clarity. (*a*) Three shell bands with high, medium and low Mn concentrations in lake sample AS07LS0026 are compared to detect speciation differences with the metal concentration; beam size on the sample was 100 μm × 50 μm. (*b*) A high Mn concentration band in the juvenile shell section and one in the adult section of the same specimen are compared to detect possible differences in Mn speciation related to ontogeny; beam size on the sample was 100 μm × 50 μm. (*c*) Spectra from Mn-rich bands in an adult shell area of the river (AS07RM0018) and the lake (AS07LS0026) sample were compared to detect possible differences owing to living environment; beam size on the sample was 100 μm × 50 μm. (*d*) A fraction of a Mn-rich aragonite crystal and a sample of a *Diplodon* periostracum were analyzed as pure inorganic and organic reference samples and compared with a shell spectrum of sample AS07LS0026 acquired under the same conditions (beam size on the sample was 350 μm × 200 μm, 3 s acquisition time). Line *a* in (*d*) marks the white line of the Mn *Kα* edge (at 6552 eV) and line *b* shows the position of the secondary peak at 6564 eV in the shell spectrum.

stracum of *Unio novahollandae*. However, the Mn-dioxide XANES spectrum (Fig. 4*a*) displays a further peak at 6578 eV (arrow) which is neither observed in the periostracum (Fig. 3*d*) nor the shell spectrum (Fig. 4*a*) of *Diplodon* and discounts a significant contribution of Mn(IV) in *Diplodon chilensis patagonicus*.

Farges (2005) showed that the correlation between redox state and Mn *K*-edge position (measured at the maximum of the white line) is not accurate enough to be quantitative, the pre-edge features being a better indicator of the speciation state. However, the presence of significant amounts of Mn(III), Mn(IV) and Mn(VII) can be excluded by comparison with other Mn organic and inorganic references with different Mn oxidation states (Table 1 and Fig. 4). The first derivative spectrum of the shell (Fig. 4*b*) shows a prominent wide peak at 6548 eV. In contrast, the Mn(IV) (Mn-dioxide) and Mn(III) (Mn-porphine) spectra differ considerably, having more than one intense peak in the same energy range. The spectrum of Mn(VII) (potassium permanganate) shows an intense pre-edge peak at 6543 eV (Fig. 4*c*) which is not observed in the shell spectrum.

The position of the white line at the Mn *K*-edge in the shell spectrum (Figs. 4*a* and 4*b*) coincides with those of all reference compounds with Mn(II). The position and the intensity of the pre-edge peak (Fig. 4*c*) in the shell spectrum (grey line) is identical to that of Mn(II), but distinctly different from compounds bearing Mn in different oxidation states. This indicates that the most likely oxidation state for Mn in the shell is Mn(II) while contributions of more oxidized Mn species cannot be ascertained.

Two of the bivalent Mn reference compounds analyzed here (Fig. 4*a*) show a secondary peak near 6564 eV (*c* in Fig. 4*a*): the $MnCO_3$ reference sample (calcite structure) at ∼6562 eV and the $MnSO_4$ sample with a shoulder at ∼6564 eV. However, the shell spectrum displays a smooth flat region above 6564 eV (beyond *c* in Fig. 4*a*) that is not well represented in the reference samples. This suggests that Mn in the shell sample has not exactly the same near-neighbour structure as in these reference materials.

Although spectroscopic studies have shown that the nacre of these shells consists of aragonite (Soldati *et al.*, 2009), this does not exclude the presence of, for example, Mn in calcite-

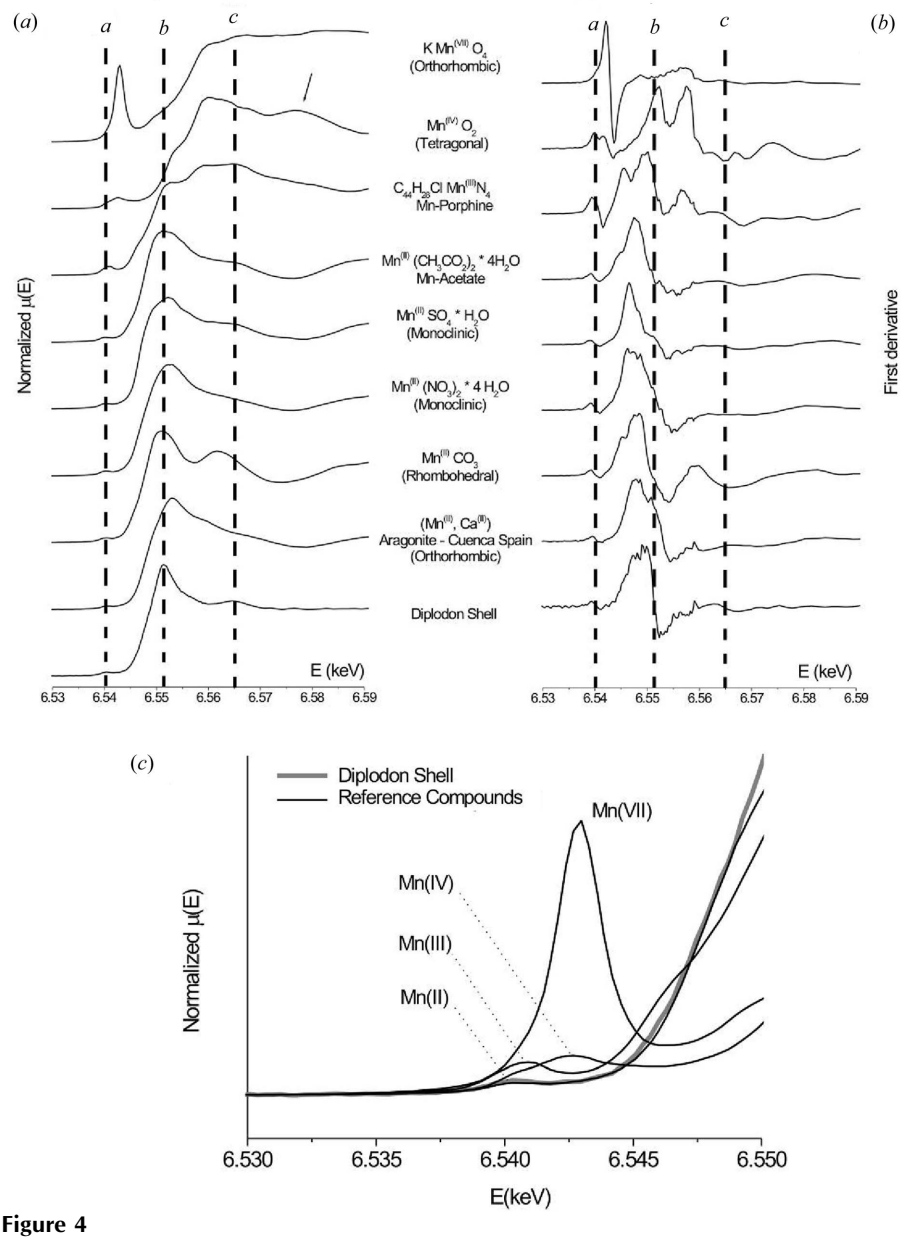

Figure 4
X-ray absorption spectra (*a*) and first derivatives (*b*) of different organic and inorganic reference materials. The spectra are normalized between 0 and an edge jump of 1 and shifted vertically for clarity. *Diplodon* shell (AS07LS0026) and aragonite crystal were measured *in situ* with an acquisition time of 3 s; the other materials were measured as powder pellets with an acquisition time of 1 s; beam size on the samples were 350 μm × 200 μm. Line *a* in (*a*) marks the position of the Mn *Kα* pre-edge peak and line *b* shows the white line of the Mn *Kα* edge of the shell spectrum (at 6552 eV). Line *c* marks the secondary peak after the white line at 6564 eV in the shell spectrum. The arrow in (*a*) points to a prominent peak at 6578 eV in the MnO_2 spectrum. (*c*) Close-up of the pre-edge region for reference substances with different oxidation states of Mn [aragonite: Mn(II); Mn-porphine: Mn(III); Mn-dioxide: Mn(IV); potassium permanganate: Mn(VII)] compared with the shell spectrum. The intensity and position of the pre-edge peak in the *Diplodon* shell spectrum corresponds best to that of Mn(II), while the peak in the spectra of the other reference compounds is shifted to higher energies.

like micro-domains. Furthermore, orientations may play a role because measurements were carried out *in situ*, and crystallites in shells are usually arranged along specific crystallographic axes (Schmahl *et al.*, 2004). For example, the angular dependence of the X-ray absorption coefficient (owing to the horizontal polarization of the synchrotron radiation) in biogenic calcite was shown to depend highly on the crystallographic orientation of the calcite and results in anisotropic XANES spectra (Pérez-Huerta *et al.*, 2008). Since we have measured in only one orientation, such effects will have to be verified in future measurements. However, anisotropy in XAS spectra will lead only to an enhancement or attenuation of resonances, but cannot explain the peak shift of about 1.2 eV of the white line between the shell spectra and aragonite, which could be an effect of more distant neighbours around the Mn atom (Farges, 2005).

In a previous work (Soldati *et al.*, 2009) it was shown that highly concentrated Mn and S areas in *Diplodon chilensis patagonicus* shells overlap on the micrometre scale. The presence of sulfur components in the organic matrix of bivalve shells has long been known (*e.g.* Wada, 1980). Sulfur linked to amino acids, for example, are found forming part of the intra-crystalline organic matrix, while acidic sulfated sugars are often contained in the central part of the insoluble inter-crystalline organic matrix (Dauphin *et al.*, 2003). Although the existence of Mn associated with SO_4^{2-} from the shell organic material is therefore plausible, this is clearly not supported by our XANES measurements. Although the pre-edge peak and white line of the Mn *Kα*-edge are positioned at similar energy (Fig. 4*a*), the first derivative spectra show distinct differences in shape, width and position of the main resonance peak between $MnSO_4$ and shell (*b* in Fig. 4*b*).

4. Conclusions

Comparing the XANES spectra of manganese in shell nacre of *Diplodon chilensis patagonicus* with those containing Mn in different oxidation states and coordination, it was found that the oxidation state of Mn in the shells is most probably Mn(II). This conclusion is based mainly on the similarity of position and intensity of the pre-edge peak and position of the white line of the main resonance peak between the shell spectra and those of Mn(II)-bearing reference compounds. Furthermore, it could be shown that provenance, ontogenetic age, concentration or seasonal deposition do not influence the speciation of manganese in this bivalve species. Although Mn concen-

trations in the high Ca-environment within *Diplodon* shells typically lie below the weight percentage range and the regions of interest are only some 100 μm in size, the sensitivity of the measurements was well above the limits of detection at the SUL-X beamline.

None of the reference spectra adopted resembles that of the shells close enough to clearly identify the Mn(II) atom neighbourhood. Despite the fact that the shell nacre is an aragonitic material, all analyzed shell samples show an increase of absorption intensity at ∼6564 eV, contrary to Mn atoms forming a solid solution in an aragonite structure or to those being hosted by the organic shell components. Other associations, such as $MnCO_3$ (calcite structure) micro-domains, appear possible. Spectral differences owing to the crystal orientation in the shell and in the aragonite mineral could not be excluded, because the measurements were carried out *in situ*. Future work should comprise XANES/EXAFS analyses at higher spatial resolution combined with modelling of organic/inorganic mixtures at the micro–nano scale to clarify the atomic position of Mn within shells of these freshwater bivalves.

This work was financed by a research fund for young scientists from the Johannes Gutenberg-University for the project 'Climate archives in biominerals (*Diplodon chilensis*) from Patagonia–Argentina' and is publication No. 619 from the Earth System Cycles Research Centre. The authors are grateful to the authorities of the National Park Nahuel Huapi for allowing sampling and to Adam Hajduk and Maria M. Bianchi who lent logistic and scientific support in Argentina. We acknowledge ANKA for granting beam time under the proposal ENV-94, Ralph Steininger from the Institute for Synchrotron Radiation for introduction to the beamline handling, and Jochen Geck (Leibniz Institute for Solid State and Materials Research, Dresden) for help with the data evaluation and interpretation. The authors are grateful to Joachim Huth (Particle Chemistry Department, Max-Planck Institut für Chemie Mainz) and Richard Wirth (Geo-Forschungs-Zentrum, Potsdam) for their valuable support in obtaining the scanning electron microscopy and transmission electron microscopy images, respectively. Reviews from Roberto Terzano and three anonymous reviewers helped to improve the manuscript and are greatly appreciated.

References

Allen, J. A. (1960). *Nature (London)*, **185**, 336–337.
Anthony, J. L., Kesler, D. H., Downing, W. L. & Downing, J. A. (2001). *Freshwater Biol.* **46**, 1349–1359.
Barbin, V., Brand, U., Hewitt, R. A. & Ramseyer, K. (1995). *Geobios*, **28**, 701–710.
Boycott, A. E. (1921). *Naturalist*, **6**, 209–211.
Bradley, H. C. (1910). *J. Biol. Chem.* **8**, 237–249.
Carré, M., Bentaleb, I., Bruguier, O., Ordinola, E., Barrett, N. T. & Fontugne, M. (2006). *Geochim. Cosmochim. Acta*, **70**, 4906–4920.
Carriker, M. R., Palmer, R. P., Sick, L. V. & Johnson, C. C. (1980). *J. Exp. Mar. Biol. Ecol.* **46**, 279–296.
Carriker, M. R., Swann, C. P. & Ewart, J. W. (1982). *Mar. Biol.* **69**, 235–246.
Castellanos, Z. A. (1959). *1° Cong. Sudam. Zool.* **1**, 85–94.
Castellanos, Z. A. (1960). *Secret. Agric. Public. Misc.* **421**, 1–40.
Clarke, L. J., Finch, A. A., Huthwelker, T., Foster, L. C., Kennedy, H. A., Richardson, C. A. & Steaggles, H. (2009). *Geophys. Res. Abs.* **11**, 9011-1.
Comfort, A. (1951). *Biol. Rev.* **26**, 285–301.
Dauphin, Y., Cuif, J.-P., Doucet, J., Salomé, M., Susini, J. & Williams, C. T. (2003). *J. Struct. Biol.* **142**, 272–280.
Dodd, J. R. (1967). *J. Paleontol.* **41**, 1313–1329.
Erben, H. K. & Watabe, N. (1974). *Nature (London)*, **248**, 128–130.
Farges, F. (2005). *Phys. Rev. B*, **71**, 155109.
Foster, L. C., Finch, A. A., Allison, N., Andersson, C. & Clarke, L. J. (2008). *Chem. Geol.* **254**, 113–119.
Fox, D. L. (1966). *Physiology of Mollusca*, Vol. 2, edited by K. M. Wilbur and C. M. Yonge, pp. 249–274. New York, London: Academic Press.
Freitas, P. S., Clarke, L. J., Kennedy, H. & Richardson, C. A. (2009). *Biogeosciences*, **6**, 1209–1227.
Freitas, P. S., Clarke, L. J., Kennedy, H., Richardson, C. A. & Abrantes, F. (2006). *Geochim. Cosmochim. Acta*, **70**, 5119–5133.
Gillikin, D. P., Dehairs, F., Lorrain, A., Steenmans, D., Baeyens, W. & André, L. (2006). *Geochim. Cosmochim. Acta*, **70**, 395–407.
Gordon, C. M., Carr, R. A. & Larson, R. E. (1970). *Limnol. Oceanogr.* **15**, 461.
Haraguchi, H. (2004). *J. Anal. Atom. Spectrom.* **19**, 5–14.
Jeffree, R. A., Markich, S. J., Lefebvre, F., Thellier, M. & Ripoll, C. (1995). *Experientia*, **51**, 838–848.
Klein, R. T., Lohmann, K. C. & Thayer, C. W. (1996*a*). *Geology*, **24**, 415–418.
Klein, R. T., Lohmann, K. C. & Thayer, C. W. (1996*b*). *Geochim. Cosmochim. Acta*, **60**, 4207–4221.
Langlet, D., Alleman, L. Y., Plisnier, P.-D., Hughes, H. & André, L. (2006). *Biogeosciences*, **3**, 1453–1471.
Lazareth, C. E., Van der Putten, E., André, L. & Dehairs, F. (2003). *Estuar. Coast. Shelf Sci.* **57**, 1103–1114.
Lingard, S. M., Evans, R. D. & Bourgoin, B. P. (1992). *Bull. Environ. Contam. Toxicol.* **48**, 179–184.
Lorens, R. B. & Bender, M. L. (1980). *Geochim. Cosmochim. Acta*, **44**, 1265–1278.
Lorrain, A., Gillikin, D. P., Paulet, Y.-M., Chauvaud, L., Le Mercier, A., Navez, J. & Andre, L. (2005). *Geology*, **33**, 965–968.
Lutz, R. A. & Rhoads, D. C. (1980). *Skeletal Growth of Aquatic Organisms: Biological Records of Environmental Change*, Vol. 1, edited by D. C. Rhoads and R. A. Lutz, pp. 203–249. New York, London: Plenum Press.
Maguire, M. E. & Cowan, J. A. (2002). *Biometals*, **15**, 203–210.
Naidu, Y. N., Rao, J. L. & Lakshman, S. V. J. (1992). *Polyhedron*, **11**, 663–669.
Narasimhulu, K. V. & Rao, J. L. (2000). *Spectrochim. Acta*, A**56**, 1345–1353.
Nietubyć, R., Sobczak, E. & Attenkofer, K. E. (2001). *J. Alloys Compd.* **328**, 126–131.
Parada, E., Peredo, S., Lara, G. & Valdebenito, I. (1989). *Arch. Hydrobiol.* **115**, 563–573.
Pérez-Huerta, A., Cusack, M., Janousch, M. & Finch, A. A. (2008). *J. Synchrotron Rad.* **15**, 572–575.
Pilkey, O. H. & Goodell, H. G. (1963). *Limnol. Oceanog.* **8**, 137–148.
Queimaliños, C. P. (1997). *Int. Revue. Ges. Hydrobiol.* **82**, 147–160.
Ravel, B. & Newville, M. (2005). *J. Synchrotron Rad.* **12**, 537–541.
Rosenberg, G. D. (1980). *Skeletal Growth of Aquatic Organisms: Biological Records of Environmental Change*, Vol. 1, edited by D. C. Rhoads and R. A. Lutz, pp. 115–129. New York, London: Plenum Press.
Rosenberg, G. D., Hughes, W. W., Parker, D. L. & Ray, B. D. (2001). *Am. Malacol. Bull.* **16**, 251–261.
Rosenberg, G. D. & Jones, C. D. (1975). *Growth Rhythms and the History of the Earth's Rotation. Interdisciplinary Winter Conference on Biological Clocks and Changes in the Earth's Rotation:*

Geophysical and Astronomical Consequences, Vol. 1, edited by G. D. Rosenberg and S. Runcorn, pp. 223–241. London: John Wiley and Sons.
Schmahl, W. W., Griesshaber, E., Neuser, R., Lenze, A., Job, R. & Brand, U. (2004). *Eur. J. Mineral.* **16**, 693–697.
Schöne, B. R., Fiebig, J., Pfeiffer, M., Gelss, R., Hickkson, J., Johnson, A. L. A., Dreyer, W. & Oschmann, W. (2005). *Paleogeogr. Paleoclimatol. Paleoecol.* **228**, 130–148.
Semenas, L. & Brungi, N. (2002). *Austral. Ecol.* **12**, 29–40.
Siegele, R., Orlic, I., Cohen, D. D., Markich, S. J. & Jeffree, R. A. (2001). *Nucl. Instrum. Methods Phys. Res. B*, **181**, 593–597.
Soldati, A. L., Jacob, D. E., Schone, B. R., Bianchi, M. M. & Hajduk, A. (2009). *J. Mollusc. Stud.* **75**, 75–85.
Soldati, A. L., Jacob, D. E., Wehrmeister, U., Häger, T. & Hofmeister, W. (2007). *J. Raman Spectrosc.* **38**, 525–536.
SUL-X (2009). *ANKA Instrumentation Book 2009*, http://ankaweb.fzk.de/_file/extras/extras_download_3.pdf.
Swinehart, J. H. & Smith, K. W. (1979). *Biol. Bull.* **156**, 369.
Takesue, R. K., Bacon, C. R. & Thompson, J. K. (2008). *Geochim. Cosmochim. Acta*, **72**, 5431–5445.
Tevesz, M. J. S. & Carter, J. G. (1980). *Skeletal Growth of Aquatic Organisms: Biological Records of Environmental Change*, Vol. 1, edited by D. C. Rhoads and R. A. Lutz, pp. 115–129. New York, London: Plenum Press.
Toland, H., Perkins, B., Pearce, N., Keenan, F. & Leng, M. J. (2000). *J. Anal. Atom. Spectrom.* **15**, 1143–1148.
Urey, H. C., Lowenstam, H. A., Epstein, S. & McKinney, C. R. (1951). *Bull. Geol. Soc. Am.* **61**, 399–416.
Valdovinos, C. & Pedreros, P. (2007). *Limnologica*, **37**, 63–75.
Van der Putten, E., Dehairs, F., Keppens, E. & Baeyens, W. (2000). *Geochim. Cosmochim. Acta*, **64**, 997–1011.
Wada, K. (1980). *The Mechanisms of Biomineralization in Animals and Plants*, Vol. 1, edited by M. Omori and N. Watabe, pp. 79–92. Tokyo: Tokai University Press.
Wanamaker, A. D., Kreutz, K. J., Wilson, T., Borns, H. W., Introne, D. S. & Feindel, S. (2008). *Geo-Mar. Lett.* **28**, 359–368.